CHAPTER 3

ALPINE GLACIAL GEOMORPHOLOGIC STUDIES IN THE CENTRAL ANDES USING LANDSAT THEMATIC MAPPER IMAGES

Abstract

Satellite images are a powerful tool for geomorphic studies, but have been used far less than traditional aerial photography. In particular, the regional overview provided by Landsat Thematic Mapper (TM) images is extremely valuable for studying late Pleistocene glaciation in the central Andes. The semiarid character of the region is conducive to the preservation and identification of moraines and other glacial geomorphic features. A Landsat TM mosaic of the central Andes was created and used to map the extent of nearly 11,000 late Pleistocene glaciers. These glaciers were larger and more numerous than their modern counterparts. At their maximum, glaciers in this region covered approximately 29,800 km^2 and had a total volume of approximately 3700 km^3. Using the "toe-to-headwall altitude ratio" (THAR) method, the equilibrium line altitude (ELA) of each paleo-glacier was calculated. Modern and late Pleistocene ELAs exhibit a similar northeast to southwest rise in elevation that is a response to decreasing precipitation across the region. The pattern of ELA depression was found to vary considerably from the uniform 1000 m lowering often assumed for tropical latitudes. In particular, the presence of high plateaus imposes a non-climatic constraint on glacial expansion.

Introduction

Aerial photography has long enjoyed widespread use in glacial geomorphic studies. Satellite remote sensing, however, has not been nearly so common. Limited usage of satellite images can be attributed to its lower spatial resolution, a perception that satellite images are not suitable for undertaking serious science (Aber *et al*., 1993), and the expense of satellite images and associated computer hardware and software necessary for image processing. However, limitations in application of satellite remote sensing for glacial geomorphic studies, such as high cost and low spatial resolution, are rapidly diminishing. At present, archives of Landsat Multispectral Scanner (MSS) at least two year old and Thematic Mapper (TM) images at least ten years old are again publicly available at reasonable costs for academic research. The upcoming Landsat 7 and EOS ASTER instruments will provide 10-15 m resolution images at low cost in the near future. The increasing power of personal computers and the wide selection of commercial and non-commercial image processing software now available for personal computers allow sophisticated image processing and analysis to be accomplished quite inexpensively.

Satellite images remains unequaled in their ability to provide a regional-scale view of the landscape. They serve both as an excellent basemap for regional studies of alpine glaciation and as a means of placing local field studies within their regional context. The central Andes of Bolivia,

southern Peru, and northern Chile are an excellent area to demonstrate the utility of Landsat TM and MSS images for glacial geomorphic mapping in an alpine environment. While some detailed field studies have been conducted in the region (e.g. Argollo, 1980; Seltzer, 1992), the inaccessibility of many glaciated areas makes it difficult develop a comprehensive regional picture of late Pleistocene glaciations using traditional field methods. Consequently, regional studies of late Pleistocene glacial extent and snowline elevation (Hastenrath, 1971; Nogami, 1976; Satoh, 1979) are based on limited observations. However, the region's semiarid to arid climate makes it extremely amenable to glacial geomorphic studies using the moderate resolution Landsat TM (28.5 m) and MSS (79 m) sensors. Well preserved moraines and other geomorphic features mark the maximum extent of late Pleistocene glaciers (Seltzer, 1992) and can be easily identified on Landsat images (Fox, 1993).

Satellite images, particularly from the Landsat series satellites, have been applied to identification of glacial geomorphic features in a variety of settings (e.g. Aber *et al*., 1993; Williams, 1986). Even using small scale (1:500,000) photographic products, it was possible to map the extent of late Pleistocene glaciation the mountains of Afghanistan (Porter, 1985). Use of digital satellite images and image processing techniques allow Landsat images to be effectively employed in mapping glacial geomorphic features at much larger scales of up to 1:50,000.

Using simple image processing techniques, a comprehensive mosaic of twenty-two Landsat Thematic Mapper scenes, covering the central Andes from 15°-22° S, was constructed. The mosaic served two purposes. The first was to allow compilation of the paleo-glaciers mapped between 18° and 22° S by Fox (1993) into a single geographic information system (GIS) coverage for analysis. The second use was to extend the moraine mapping northward to 15° S. This additional mapping doubled the number of paleo-glaciers in the central Andes identified using Landsat images. In all, the Landsat mapping revealed that approximately 11,000 paleo-glaciers occupied the region during the late Pleistocene. Combining the mapping and topographic information, the areas and volumes of these former glaciers were estimated. The equilibrium line altitude (ELA) of each individual paleo-glacier was also determined, yielding the spatial distribution of late Pleistocene ELAs over the region in considerable detail.

Study Area

This study encompasses the Peruvian-Bolivian Andes between 15° S and 22° S (**Figure 3.1**). At these latitudes, the Andes are divided into an eastern and a western cordillera both of which support modern glaciers. The cordilleras are separated by a large intermontane internally-drained basin of high elevation but low relief known as the Altiplano. This plateau is second only to the Tibetan Plateau in height and area.

Figure 3.1: Topography of the central Andes shown as greyscale (Defense Mapping Agency, 1989; Isacks, 1988)

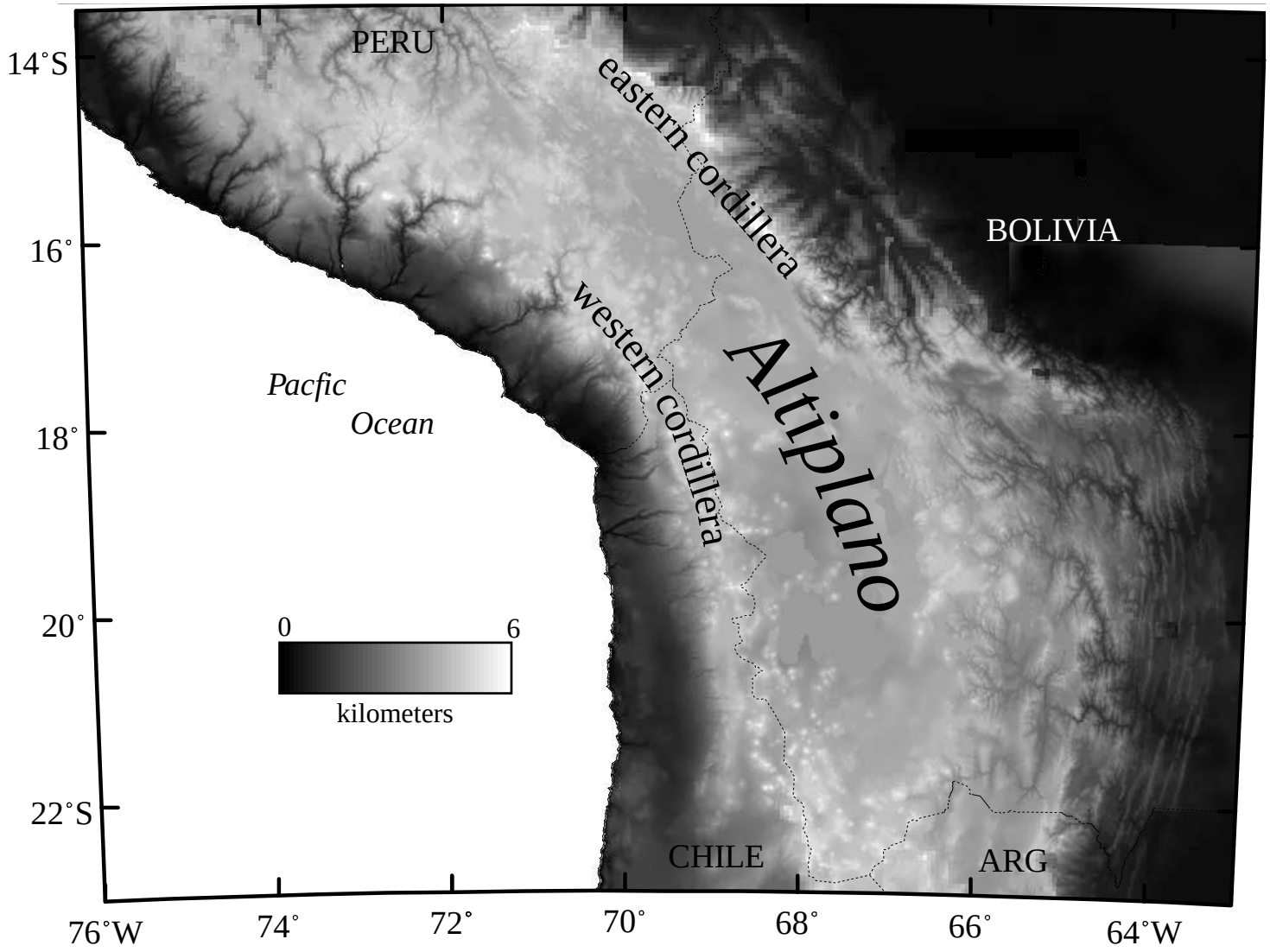
PERU
BOLIVIA
CHILE
ARG
eastern cordillera
western cordillera
Altiplano
Pacfic
Ocean
0
6
kilometers
14˚S
16˚
18˚
20˚
22˚S
76˚W
74˚
72˚
70˚
68˚
66˚
64˚W

The ages of the late Pleistocene glacial features in the region are difficult to constrain because nearly all late Pleistocene glacial dates give only minimum age for deglaciation (Seltzer, 1990). Dates from several sites in the tropical Andes suggest that glaciers reached their maximum extent prior to 20,000 ^{14}C yr BP (Mercer, 1984; Seltzer, 1992; Wright, 1983), but the exact timing is still uncertain. In this study, the glacial chronology of the central Andes is not of primary interest. However, it is assumed that all glacial features identified as late Pleistocene age formed contemporaneously. As the regional glacial chronology continues to improved, this assumption may be found to be incorrect. At present, however, the paucity of glacial dates makes it impossible to either confirm or refute this assumption.

The climate of the central Andes is characterized by a lack of significant thermal seasonality and a predominance of the diurnal temperature cycle. Precipitation provides the primary seasonal climate signal in the region. The region has a wet-dry climate associated with the north-south migration of the Intertropical Convergence Zone (ITCZ). A single rainy season extends from October to March. During the remainder of the year, the region receives very little precipitation.

Precipitation, even for the extreme westerly portions of the region, is derived from Atlantic moisture that has been transported from the east across the South American lowlands. The regional precipitation pattern shows an northeast-southwest decrease in precipitation from the Amazon lowlands (~2000 mm) to the Chilean coast (< 200 mm). Superimposed on

this regional decrease are local orographic precipitation extremes occurring on lower eastern Andean slopes. The region's semiarid and prolonged dry season are excellent for remote sensing studies as atmospheric conditions during the dry winter months are commonly clear and cloudless.

Image Processing

Image processing and geographical information systems (GIS) software were used to map, compile, and analyze the late Pleistocene glacial landforms of the central Andes mapped from Landsat images. Before the images were used for mapping, steps were taken to produce a uniform and geographically referenced mapping base. While the radiometric and geometric correction of satellite images is an arduous task, it is necessary if satellite images are to be combined with other geographic information in a geographical information system.

Radiometric corrections

In combining Landsat scenes acquired on different dates and under varied atmospheric conditions it is necessary to calibrate the images radiometrically (Lillesand and Kiefer, 1987). Radiometric calibration reduces variations in color among scenes. In the semiarid to arid environment of Bolivia, simple radiometric corrections do an excellent job in compensating for illumination and atmospheric changes and allowed multiple images to be merged without unsightly or distracting color contrasts between the scenes. Radiometric calibration also preserves the relative band to band spectral

information so that image spectra can be compared to laboratory or field spectra (Robinove, 1982) and so computer classification of modern snow cover can be performed.

The individual pixels of a Landsat TM and MSS images are quantized into a number of discrete values called digital numbers or DN values. Radiometric correction, discussed in detail by Robinove (1982) and Markham and Barker (1986) and outlined here, involves converting the raw DN values to spectral radiances or reflectances. The first step in radiometrically processing a Landsat TM or MSS image requires converting the raw DN values into units of in-band spectral radiance received at the satellite:

$$L_l = L_{\min\, l} + \left(\frac{L_{\max\, l} - L_{\min\, l}}{DN_{\max}} \right) DN \qquad (1)$$

where L_λ is the spectral radiance in mW cm^{-2} $ster^{-1}$ μm^{-1}, $L_{min\lambda}$ is the spectral radiance at DN = 0, $L_{max\lambda}$ is the spectral radiance at DN = DN_{max} where DN_{max} is 255 for 8 bit TM data , 127 for 7 bit MSS data, and 63 for 6 bit MSS data. Values for $L_{min\lambda}$ and $L_{max\lambda}$ used in the TM corrections can be found in **Table 3.1** or in Markham and Barker (1986). The values of the first (offset) and second (gain) terms in the equation are also located in the ancillary information files on the Landsat image tapes.

In addition to converting the DN values in each band to a spectral radiance, corrections were made to compensate for varying illumination between scenes acquired at different times of the year and for differences in

Table 3.1: Values for L_{min} and L_{max} used in processing Landsat Scenes in the central Andes. These are the of L_{min} and L_{max} for TM scenes processed after January 15th, 1984 and correspond to the acquisition dates of most of the images employed in this study. Values of L_{min} and L_{max} for TM scenes processed before this date and values for MSS images can be found in Tables 1 and 2 of Markham and Barker (1986).

Band	L_{min}	L_{max}
1	-0.15	15.21
2	-0.28	29.68
3	-0.12	20.43
4	-0.15	20.62
5	-0.037	2.719
6	0.1238	1.5600
7	-0.015	1.438

solar irradiance between bands (Robinove, 1982). This is accomplished by converting the solar radiances (equation 1) to effective at satellite reflectance, or in-band planetary albedo (ρ_p).

$$r_p = \frac{pL_l d^2}{E_{sun}\cos(q_z)} \quad (2)$$

where ρ_p is the unitless effective at-satellite planetary albedo, L_λ is the spectral radiance, d is the earth sun distance in astronomical units (approximately 1.0), E_{sun} is the mean solar exoatmospheric spectral irradiance (mW cm^{-2} um^{-1}), and θ_z is the solar zenith angle at the time of image acquisition. The values for E_{sun} are given in **Table 3.2**, values for θ_z are found in the ancillary files. Daily earth-sun distances can be found in *The Astronomical Almanac* published by the United States Naval Observatory.

It is also necessary to correct satellite images for atmospheric effects as the radiance received at the satellite sensor includes both surface and atmospheric components. The atmosphere affects electromagnetic radiation by scattering, absorption, and refraction. Scattering processes dominate (Slater *et al.*, 1983) of which Rayleigh and Mie types are the most common. Rayleigh scattering occurs when radiation interacts with particles of much smaller diameter than the wavelength with the scattering inversely proportional to the fourth power of the wavelength (λ^{-4}). Mie scattering occurs when propagating electromagnetic radiation encounters particles with

Table 3.2: Landsat Thematic Mapper Solar Exoatmospheric Spectral Irradiances (mW cm^{-2} μm^{-1}). Values in this table are taken from Table 4 in Markham and Barker (1986).

Band	Landsat 4	Landsat 5
1	195.8	195.7
2	182.8	182.9
3	155.9	155.7
4	104.5	104.7
5	21.91	21.93
7	7.457	7.452

diameters essentially equal to that of the wavelength, and scattering is inversely proportional to the wavelength (λ^{-1}). Under typical atmospheric conditions the actual wavelength dependence of scattering conforms to neither Rayleigh nor Mie models but rather seems to vary between λ^{-2} to $\lambda^{-0.7}$ (Chavez, 1989; Slater *et al*., 1983). However, scattering in the high dry environments of the central Andes appears to be adequately modeled by a simple Rayleigh scattering model which has also been found true of other arid environments (Chavez, 1988).

Various methods of haze correction are available to remedy these atmospheric effects. Because most geomorphic applications employ previously collected images, atmospheric conditions at the time of image acquisition are seldom known. Fortunately, this is not a severe problem as most geomorphic studies are primarily interpretive in nature and do not require high radiometric precision. A simple haze correction technique known as blackbody subtraction which requires only image information is usually adequate.

Blackbody subtraction assumes that within each scene there is a high probability that at least some resolution elements or pixels will have no reflectance because of deep shadowing. In the absence of atmospheric effects these pixels should have a DN value of 0. The actual DN values in each band for these pixels therefore represents the effect of the atmosphere on the

image (Chavez, 1988). In the simplest blackbody correction this DN value for each band is subtracted from all pixels in the image.

One problem with this approach is that the selected correction values may not conform to the realistic relative atmospheric scattering models described above. This problem is avoided by using the improved dark-object subtraction method of Chavez (1988). In this method a DN value is selected in one band and a relative scattering model (usually ranging from λ^{-4} for clear conditions to $\lambda^{-0.5}$ for very hazy conditions) is used to calculate the offset in the remainder of the bands. As the shortest wavelengths (TM band 1 and MSS band 4) require the largest corrections, an offset is selected from the image for these bands and the relative scattering model is used to predict the offsets in the remainder of the bands. In the absence of changing vegetation, snow, or cloud cover, these radiometric corrections remove most distracting color contrasts among scenes and allow creation of very uniform image mosaics in semiarid to arid environments such as the central Andes.

To create a color composite suitable for visual interpretation of geomorphic and geologic features, Landsat TM bands 5 (1.55-1.75 μm), 4 (0.76-0.90 μm) and 2 (0.52-0.60 μm) were displayed as red, green, and blue respectively. This produces a pseudocolor image with good color contrast between surface materials but whose colors are similar enough to those in the visible wavelengths to be easily interpretable by individuals with little or no remote sensing expertise. In areas where hydrothermal alteration of rocks

may be important, replacing TM band 5 with TM band 7 (2.08-2.35 μm) may yield better discrimination between rock types. Finally, histogram stretching was employed to enhance the contrast in each of the displayed bands. After the above radiometric corrections have been applied, an identical stretch was applied to each scene in the mosaic and small adjustments were made only to improve the color matching between scenes affected by thin cirrus clouds.

Geometric Rectification

Combining multiple Landsat images into a single mosaic requires that each individual scene be geometrically rectified into a common map projection. This study employs a Transverse Mercator projection designed to minimize geometric distortions within the central Andes. Each image was transformed into the projection using ground control points (GCPs) which are locations whose geographic position is known and that can be located precisely within the image. Good GCP candidates are cultural features such as road intersections. However, in underdeveloped agrarian landscapes such as the central Andes, cultural features are scarce and hard to identify. Therefore, natural features such as river junctions were commonly employed as GCPs. Coefficients for two coordinate transformation equations that relate the geographic coordinates to the uncorrected image coordinates were then determined by least-squares regression (Lillesand and Kiefer, 1987). Spatial errors for most scenes were on the order of 2-2.5 pixels indicating the locational accuracy for most pixels in the final mosaic is approximately 60-75

m. A monochromatic version of the final radiometrically corrected and geometrically rectified Landsat TM mosaic of the central Andes is shown in **Figure 3.2**

Glacial geomorphic mapping

The corrected images were used to map the area encompassed by each paleo-glacier. The lower limits of each paleo-glacier were primarily identified by lateral and terminal moraines. Lateral moraines or glacial trimlines define the middle reaches of the paleo-glacier and in the upper reaches the extent of each paleo-glacier was estimated by projecting the lateral moraines or trimlines to the glacier headwall. Approximately 11,000 paleo-glaciers were mapped in this manner.

In much of this semiarid region, glacial geomorphic features are well preserved and easily discernible on both TM and MSS images (**Figure 3.3**). The higher spatial resolution and increased spectral content of TM make it superior to MSS for identification of alpine glacier features. Identification of glacial features on the more humid and vegetated eastern slopes of the eastern cordilleras in Bolivia and portions of southwestern Peru was more difficult. Both areas have extremely high relief. Although modern glaciers are confined to the peaks, late Pleistocene glaciers descended in narrow valleys to much lower elevations. In portions of the eastern cordillera, SPOT panchromatic (10 M) images and aerial photography were used as a check on the TM mapping. Many of the glacial features resolved in the SPOT images

Figure 3.2: Landsat Thematic Mapper mosaic of the central Andes with band 4 shown in grayscale.

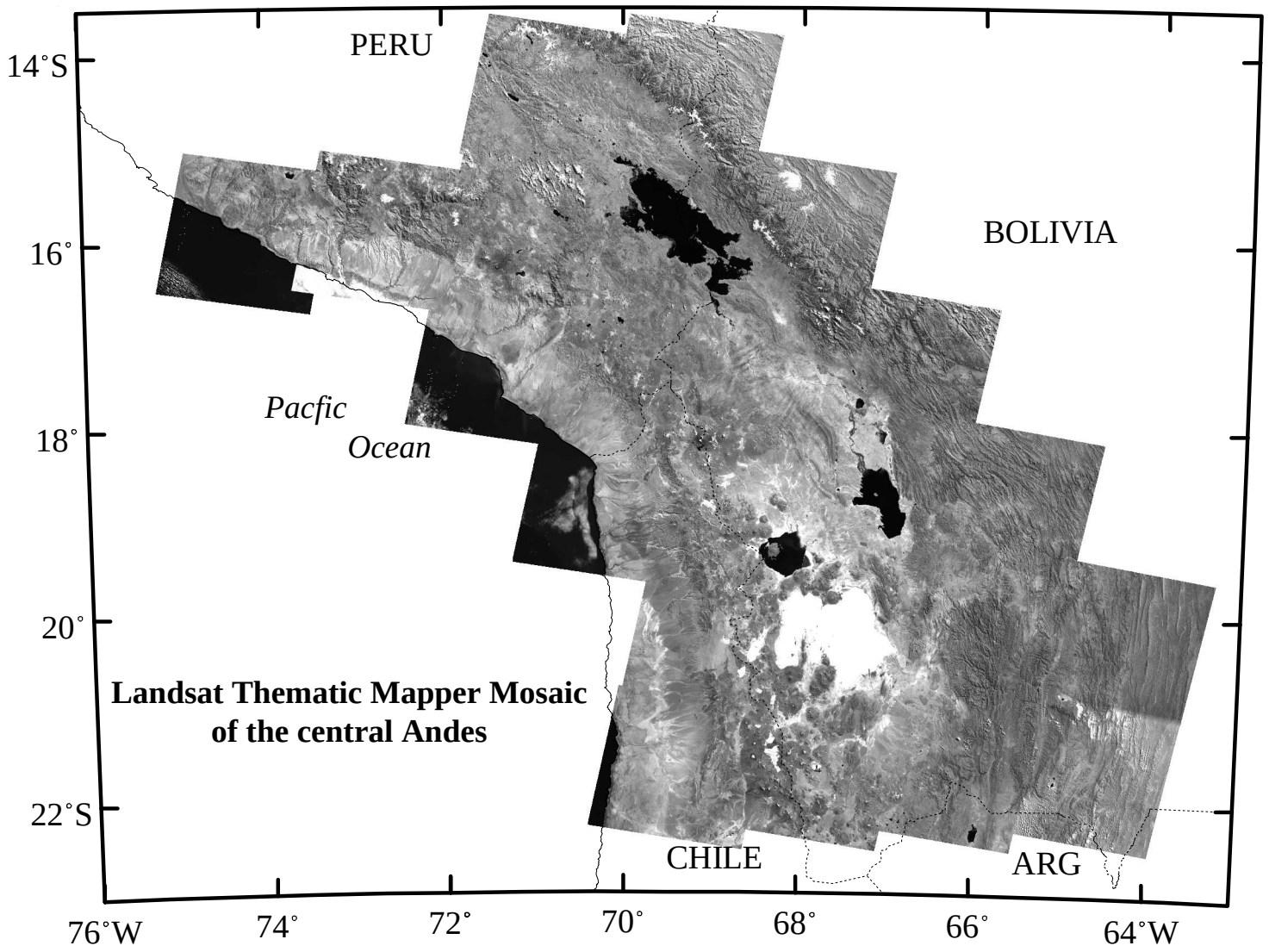
PERU
BOLIVIA
Pacfic
Ocean
CHILE
ARG
Landsat Thematic Mapper Mosaic
of the central Andes
14˚S
16˚
18˚
20˚
22˚S
76˚W
74˚
72˚
70˚
68˚
66˚
64˚W

Figure 3.3: Monochromatic (TM band 4 and MSS band 7) example showing an example of moraine identification using Landsat Thematic Mapper (left) and Landsat Multispectral Scanner images (right) for Nevado Sajama, Bolivia. The white outline represents the extent of late Pleistocene glaciers mapped using TM. While the moraine crests are quite sharp in the TM image, the are not nearly as well defined in the lower resolution MSS image (insets).

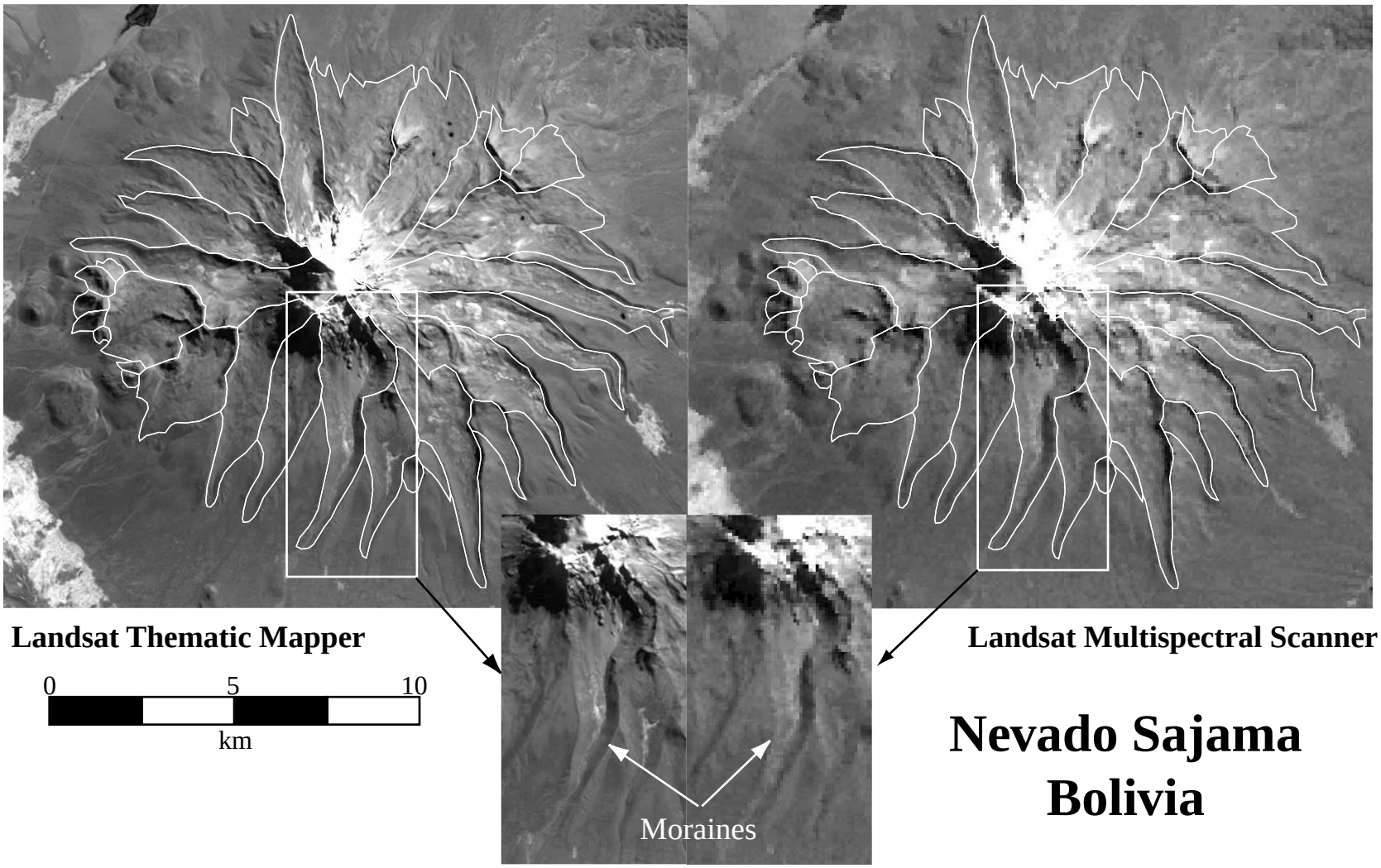
Landsat Thematic Mapper
Landsat Multispectral Scanner
0
5
10
km
Moraines
Nevado Sajama
Bolivia

and aerial photographs could also be identified in the TM although they were less well defined (**Figure 3.4**). The glacial extents visible on these higher resolution images closely matched those mapped using TM images, lending confidence to our TM based interpretations.

The altitude of the equilibrium line of each paleo-glacier was estimated using a Toe-to-Headwall Altitude Ratio or THAR (Meierding, 1982) of 0.45. The choice of 0.45 as a representative THAR value is discussed in detail in Chapter 2.

The minimum (toe) and maximum (headwall) elevations used with the THAR to estimate the ELA of each paleo-glacier were determined by overlaying the glacial extents on 1:50,000, 1:100,000, or 1:250,000 topographic maps (produced by the Instituto Geografia Militar, in La Paz, Bolivia and Lima, Peru) and recording the minimum and maximum elevations within the mapped paleo-glacier.

Modern snow cover classification

In addition to use as a geomorphic mapping base, Landsat TM was used to determine the area of the central Andes covered by modern glaciers and snow cover. Snow covered areas were determined using the snow cover classification algorithm developed by Dozier (1989). The radiometric calibration discussed previously allowed a uniform classification criterion to determine if a pixel contained snow. The classification criteria are as follows: reflectance in TM band 1 (0.45-0.52 μm) greater than 15%; reflectance in TM

Figure 3.4: A comparison of SPOT panchromatic (10 m) and Landsat TM (28.5) images for an small area in the rugged eastern cordillera of Bolivia. Moraines are that can be identified easily in the SPOT image (left) are less recognizable but can still be mapped in the Landsat image (right).

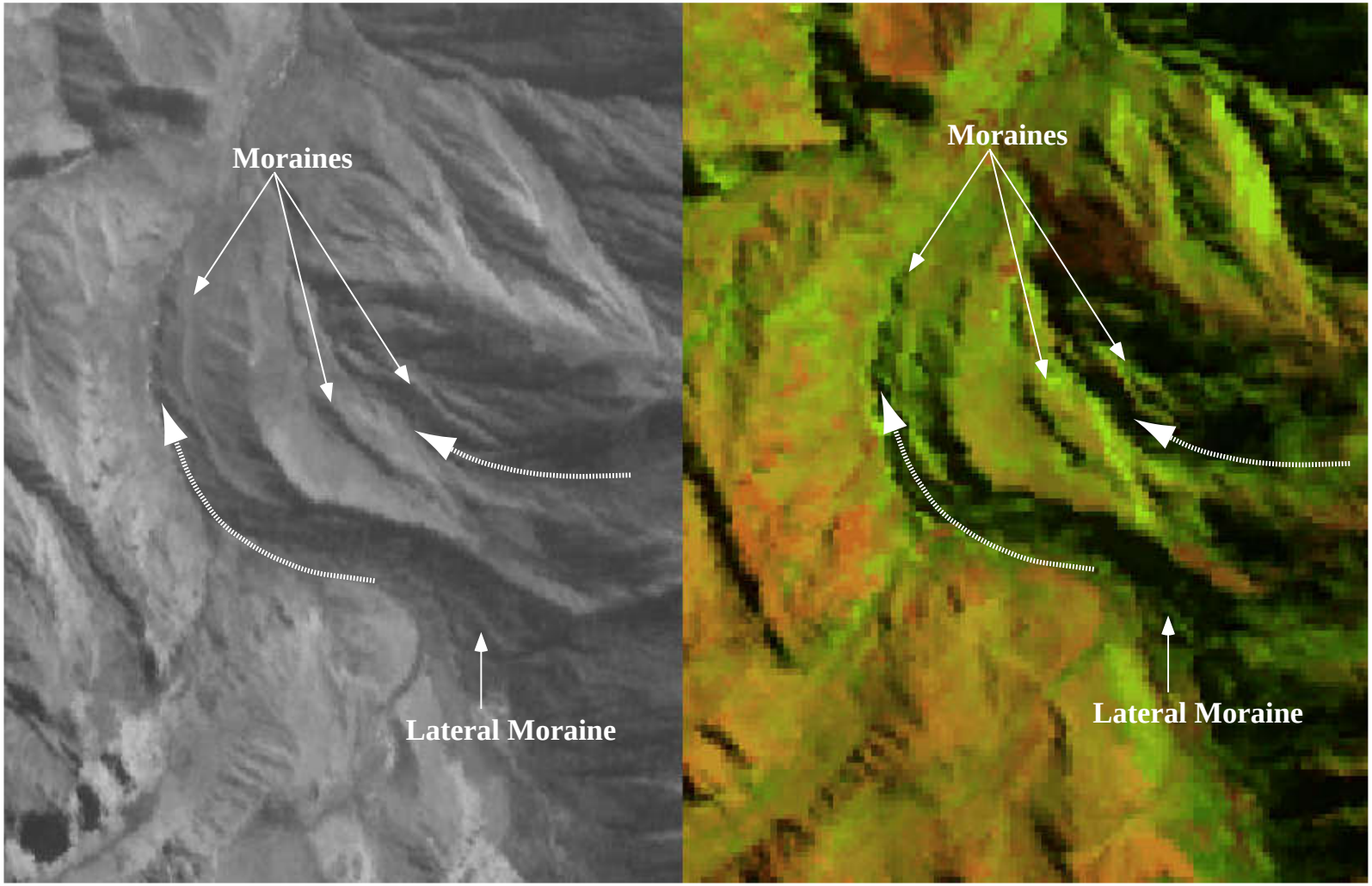

SPOT Panchromatic

0 1

km

Landsat Thematic Mapper

bands 5 4 2

band 5 (1.55-1.75 μm) less than 15%; and the normalized difference ratio between TM band 2 (0.52-0.60 μm) and TM band 5, [(TM2-TM5)/(TM2+TM5)], greater than 0.50. The areas classified as snow and glaciers are shown in **Figure 3.5**. As most of the images were collected during the dry winter months, the snow cover in the TM mosaic should be near its annual minimum. The modern snowline, which is used as a rough proxy for the elevation of the ELA, was estimated by determining the lower elevational limit of the classified snow cover. Snowline elevations were recorded every 1-2 km along the lower limit of snow cover to capture the local variability in snowline altitudes.

Glacier size and area

At their late Pleistocene maximum (**Figure 3.6**), glaciers in the central Andes between 15° and 22° S latitude occupied approximately 29,800 km^2. Based on analysis of the TM-based snow cover classification, snow and glaciers currently occupy approximately 1305 km^2 in the central Andes. As this total includes both snow and glaciers, it is an overestimation of the present glaciated area. Estimates of modern glacierized areas based on glacial inventories in Bolivia (Jordan, 1991), Peru (Hidrandina, 1988), and Chile (Oyarzun, 1987) indicate that approximately 684 km^2 of the central Andes are glaciated (**Table 3.3**). Because glacier inventories were not available for two glacierized areas in southwestern Peru, this sum underestimates the total glacierized area. These two estimates (684 km^2 and

Figure 3.5: Modern snow cover extent (black) in the central Andes calculated from the Landsat Thematic Mapper images shown in **Figure 3.2**. The large lakes and salars in the region are shown in gray.

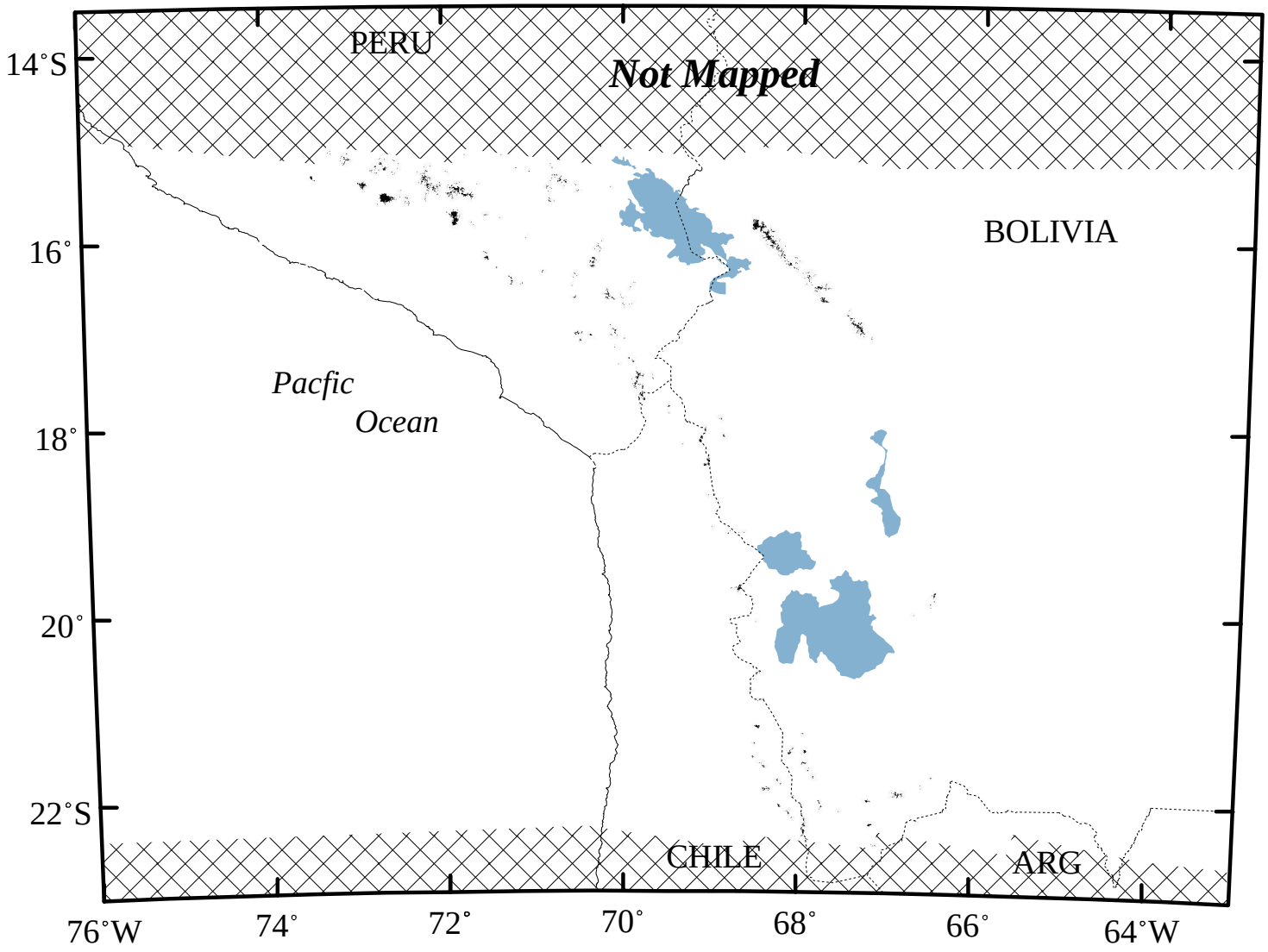
PERU
Not Mapped
BOLIVIA
Pacfic
Ocean
CHILE
ARG
14˚S
16˚
18˚
20˚
22˚S
76˚W
74˚
72˚
70˚
68˚
66˚
64˚W

Figure 3.6: late Pleistocene glacier extent (black) in the central Andes mapped from Landsat Thematic Mapper images shown in **Figure 3.2**.

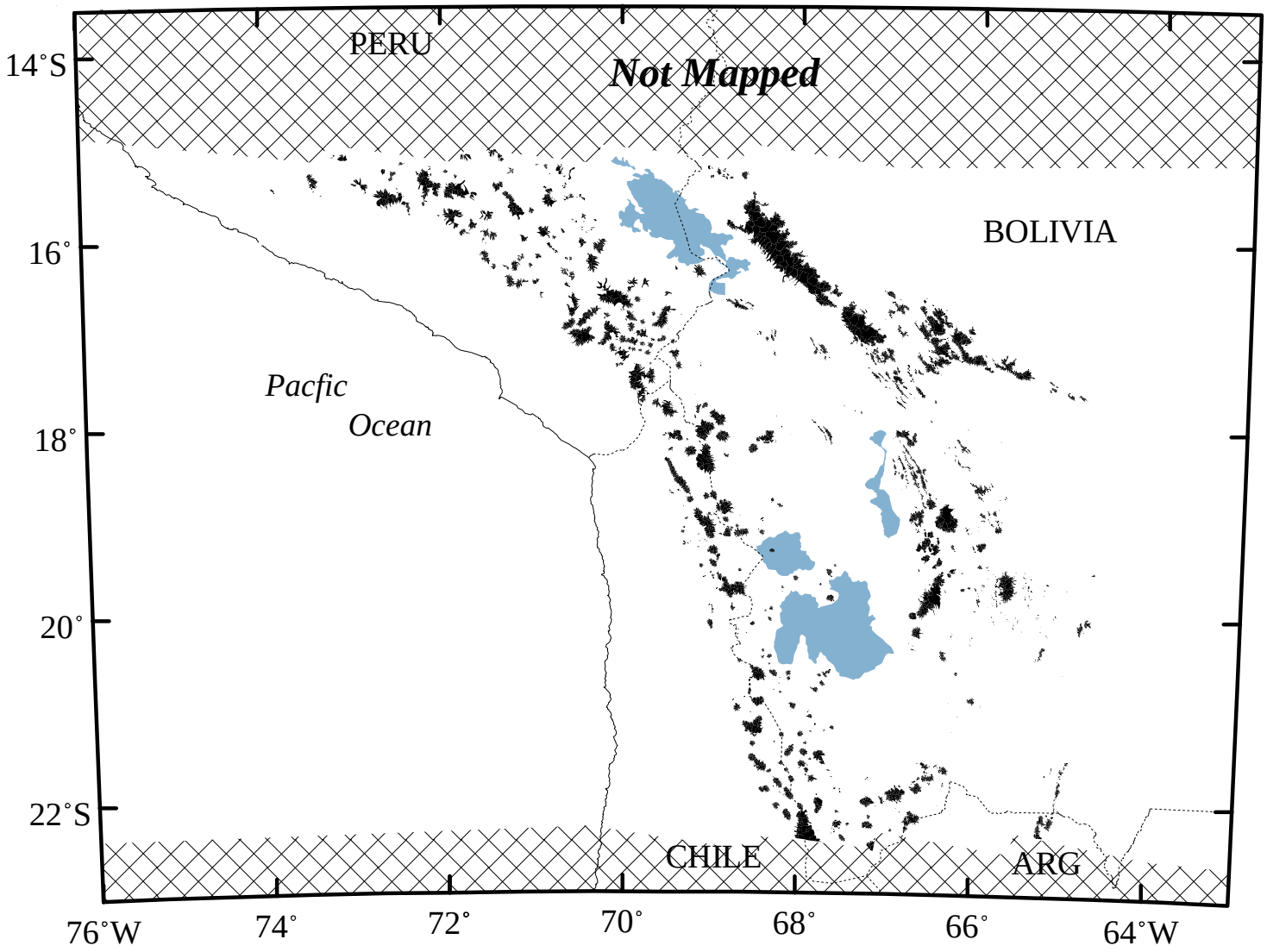
PERU
Not Mapped
BOLIVIA
Pacfic
Ocean
CHILE
ARG
14˚S
16˚
18˚
20˚
22˚S
76˚W
74˚
72˚
70˚
68˚
66˚
64˚W

Table 3.3: Number and area of modern glaciers found within the central Andes 15°-22° S.

Region	Subregion	Number	Area (km^2)
Central Andes		**1539**	**684.37**
Bolivia[1]		**1174+**	**369.72**
eastern cordillera		*1174*	*356.72*
	Cordillera de Munecas	16	0.68
	Cordillera Real	985	317.16
	Tres Cruces	156	36.65
	Santa Vera Cruz	17	2.23
western cordillera		*NA*	*13*
	Nevado Condoriri	NA	2
	Nevado Sajama	NA	4
	Nevaods Payachata	NA	5
	Mevdo Quimsa Chata	NA	2
Peru[2]		**343**	**228.82**
	Ampato	93	146.73
	Huanzo	115	36.93
	Chila	87	33.89
	La Raya	48	11.27
	Volcanica	NA	NA
	Barroso	NA	NA
Chile[3]	18°-22°S	**22**	**85.83**

[1]Jordan (1991), [2]Hidrandina (1988), [3]Oyarzun (1987)

1305 km^2) bracket the area of the central Andes covered by modern glaciers. This area is only a small fraction (2-4%) of the maximum late Pleistocene glaciated area.

At present, approximately 1500 glaciers exist in the central Andes from 15° to 22° S. The majority (1174+) are in the eastern cordilleras of Bolivia (Jordan, 1991). In the Chilean Andes between 18° and 22° S, Oyarzun (1987) inventoried 22 glaciers and the western cordilleras of Bolivia contain a few additional (Jordan, 1991). The number of glaciers existing in Peru south of 15° is unknown because of an incomplete glacier inventory in Peru. Excluding unsurveyed areas, Peruvian glaciers within the study region number approximately 340 (Hidrandina, 1988). In contrast, at the time of maximum extent, approximately 11,000 glaciers existed in the central Andes. While there is uncertainty in this estimate arising from subjective decisions made in the mapping process concerning whether individual ice masses should be split or joined, the number of late Pleistocene glaciers was nearly an order of magnitude greater than those presently existing in the central Andes. At the time of maximum extent, glaciers were considerably larger as well. The largest modern glacier within the entire Peru and Bolivia Andes is 16.5 km^2. In contrast the largest mapped LGM glacier covered an area of 264 km^2 (**Table 3.4**). Both the mean and median sizes of the late Pleistocene glaciers were larger as well, indicating an overall increase in glacier size.

Table 3.4: Area statistics of modern glaciers and Late Pleistocene paleo-glaciers in the central Andes (World Glacier Monitoring Service, unpublished data)

	Mean area (km^2)	median area (km^2)	standard deviation (km^2)	minimum area (km^2)	maximum area (km^2)	number
Peru	0.67	0.25	1.24	0.01	16.50	1,679
Bolivia	0.34	0.07	0.82	0.01	10.32	1,501
Paleo	2.72	0.87	8.01	0.001	264.31	10,941

With the exception of the smallest glaciers, a power-law relationship between glacier area and number can be demonstrated in many areas of the world (Meier and Bahr, 1995). Therefore, the area-number distributions of modern and late Pleistocene glaciers in the central Andes were examined to see if either follows a power-law relationship and to determine if the size distributions of the present and former glaciers are similar. The area-number distribution for modern glaciers was calculated from the glacier inventories of Peru and Bolivia (World Glacier Monitoring Service, unpublished data). As can be seen from the cumulative frequency plot (**Figure 3.7A**), the size distribution of modern glaciers in the central Andes does not appear to follow a power-law relationship. This is probably due to the numerous small glaciers in the region (**Table 3.4**). Only at glacier sizes greater than 1 km^2, do glacier size and number follow a power-law relationship. The normalized cumulative frequency curves (**Figure 3.7A**) of modern Peruvian and Bolivian glaciers parallel each other, indicating that while the mean sizes differ (as is shown in **Table 3.4**), their relative size distributions are similar.

The relationship between glacier size and number for late Pleistocene glaciers in the central Andes varies considerably from these modern distributions. There is little evidence, even at the largest glacier sizes, of a power-law relationship between glacier size and number. Also, the ratio of large glaciers to small ones was greater during late Pleistocene times than at present. This is what would be expected if smaller glaciers coalesced into

Figure 3.7: **(A)** a cumulative frequency plot of the size (km^2) of modern and late Pleistocene glaciers in the central Andes of Peru and Bolivia versus number (N_c). **(B)** identical to **(A)** expect each curve has been normalized by the total number of glaciers.

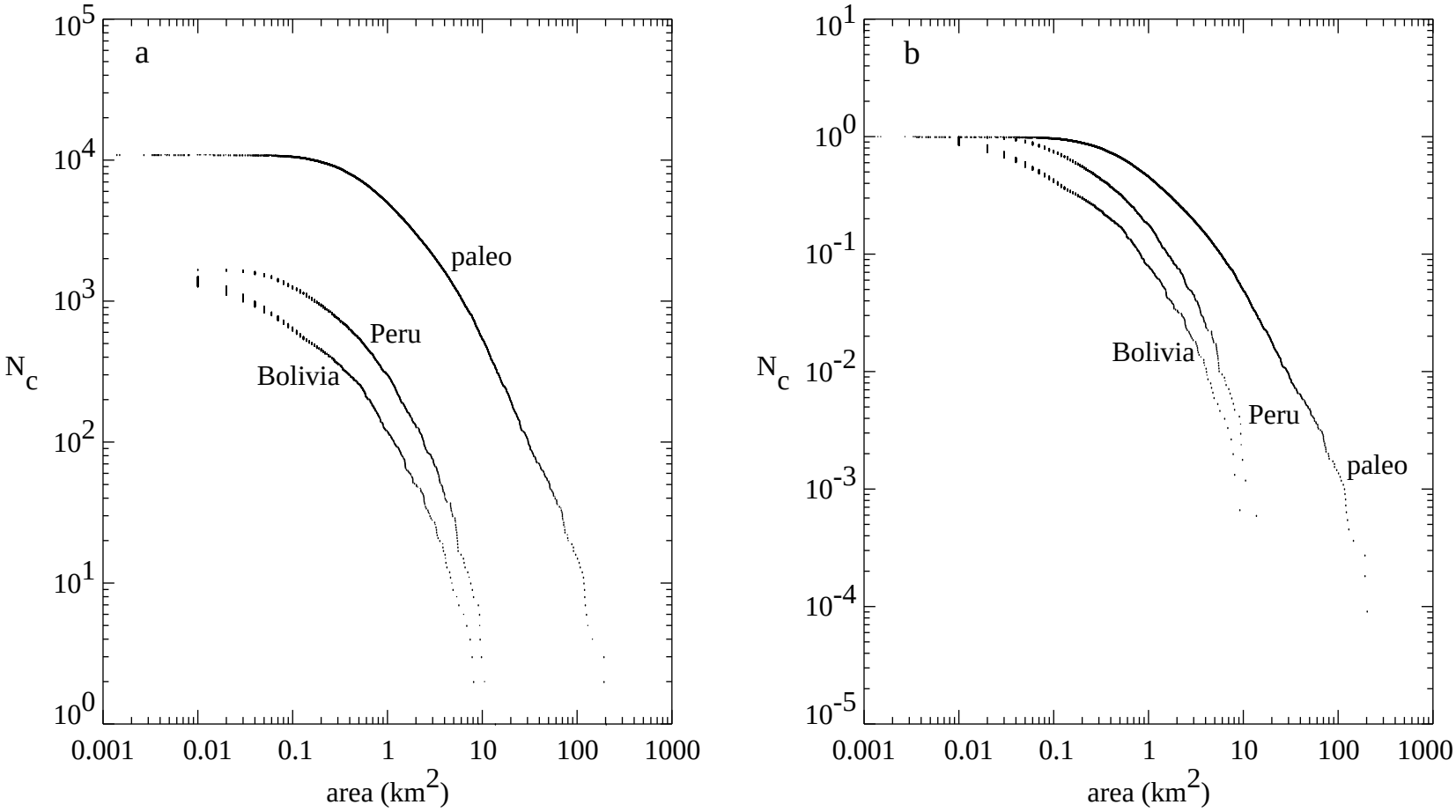
a
b
paleo
Peru
Bolivia
N_c
area (km^2)
10^5
10^4
10^3
10^2
10^1
10^0
10^1
10^0
10^{-1}
10^{-2}
10^{-3}
10^{-4}
10^{-5}
0.001
0.01
0.1
1
10
100
1000

larger glacier systems during the late Pleistocene. However, it could also be an artifact resulting from lumping small individual glaciers into larger ice bodies during the mapping process. Despite the differences in size distribution between modern and late Pleistocene glaciers, their overall similarity provides some confidence that Landsat TM-based glacier mapping is a accurate representation of late Pleistocene glaciers in the central Andes.

Ice volume of late Pleistocene glaciers

In addition to determining the size of late Pleistocene glaciers in the central Andes, it is also interesting to estimate their equivalent ice or water volume. This requires knowledge of the relationship between glacier area and volume. A statistical relationship between the area of late Pleistocene glaciers and their volume was previously developed by Fox (1993) using the sixty-nine reconstructed glaciers described above. For the entire central Andes, ice volume estimated using this relationship is 4347 km^3. However, no physical basis exists for this empirically derived relationship.

Recent empirical (Meier and Bahr, 1995) and theoretical scaling (Bahr *et al.*, 1995) studies indicate that for small modern temperate glaciers, volume scales as an exponential function of area:

$$V = cA^b \tag{3}$$

where V is volume, A is area, and c and b are scaling factors. The empirically determined exponential scaling factor (b = 1.36) has been found to have a theoretical basis (Bahr *et al.*, 1995; Meier and Bahr, 1995). The area-volume

relationship of the sixty-nine reconstructed glaciers conforms to this exponential relationship as well (**Figure 3.8**). Through least-squares curve fitting, the linear scaling term (c) was estimated to be 0.048. Equation (3) allows the total ice volume of late Pleistocene glaciers to be more confidently estimated as 3676 km^3. The large difference (15%) in ice volume estimates is caused by the greater volumes estimated for of the largest and smallest glaciers by the Fox (1993) equation.

Regional ELA pattern and depressions

The regional view of the central Andes provided by Landsat TM images has enabled reconstruction of the elevation of the late Pleistocene equilibrium line in detail and with spatial coverage not possible using traditional field methods. By comparing the regional ELA patterns of late Pleistocene glaciers with those at present, the regional pattern of ELA lowering was calculated. The amount of ELA lowering varies considerably across the central Andes and this fact has important consequences for paleoclimatic interpretations based on ELA depressions.

Both modern (**Figure 3.9**) and late Pleistocene (**Figure 3.10**) ELAs show a rise northeast to southwest across the central Andes. Modern ELA rises steeply from 4400-4500 m to over 5000 meters across the eastern cordillera of Bolivia then rises more gently across the Altiplano to extremely high elevations (>5800 m) along the Bolivia-Chile border. This rise in modern ELA is a direct consequence of decreasing precipitation across the

Figure 3.8: Area volume relationship for the sixty-nine reconstructed late Pleistocene glaciers (Fox, 1993). The solid curve is the area-volume relationship developed for modern glaciers by (Meier and Bahr, 1995). The dashed line represents the original empirical relationship determined by Fox. The curvature in the Fox (1993) relationship causes excessive volumes to be estimated for glaciers with areas outside the sampled sizes. Because many glaciers of these sizes do exist, the use of the area-volume relationship developed by Meier and Bahr (1995) is preferable.

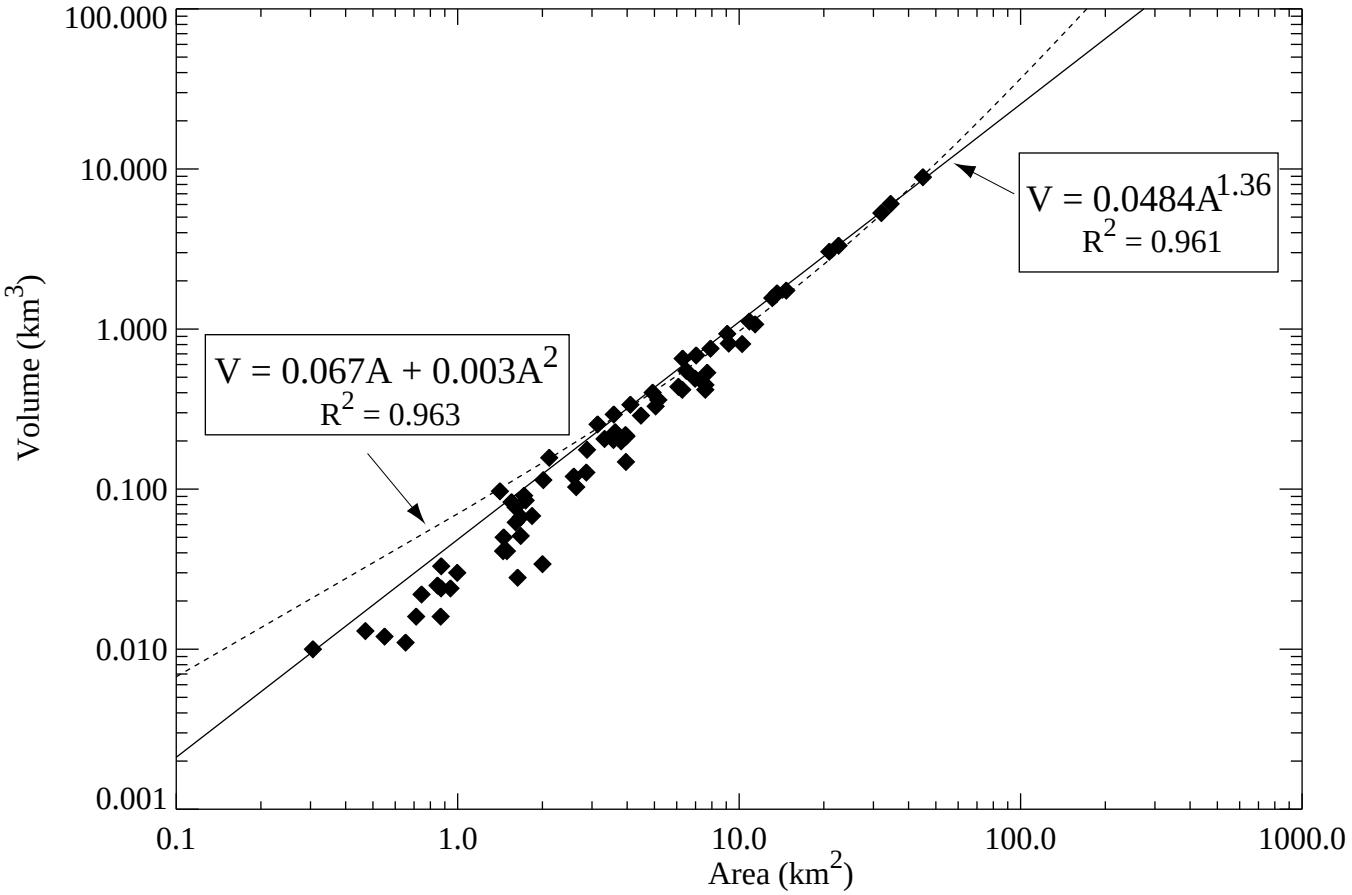
100.000
10.000
1.000
0.100
0.010
0.001
Volume (km3)
0.1
1.0
10.0
100.0
1000.0
Area (km2)
V = 0.067A + 0.003A2
R2 = 0.963
V = 0.0484A1.36
R2 = 0.961

Figure 3.9: Modern snowline elevation in the central Andes based on the classified snow cover shown in **Figure 3.5**. The contours were created by averaging individual elevation estimates in a 0.25° x 0.25° moving window and hand contouring the data grid. Contour interval is 100 m.

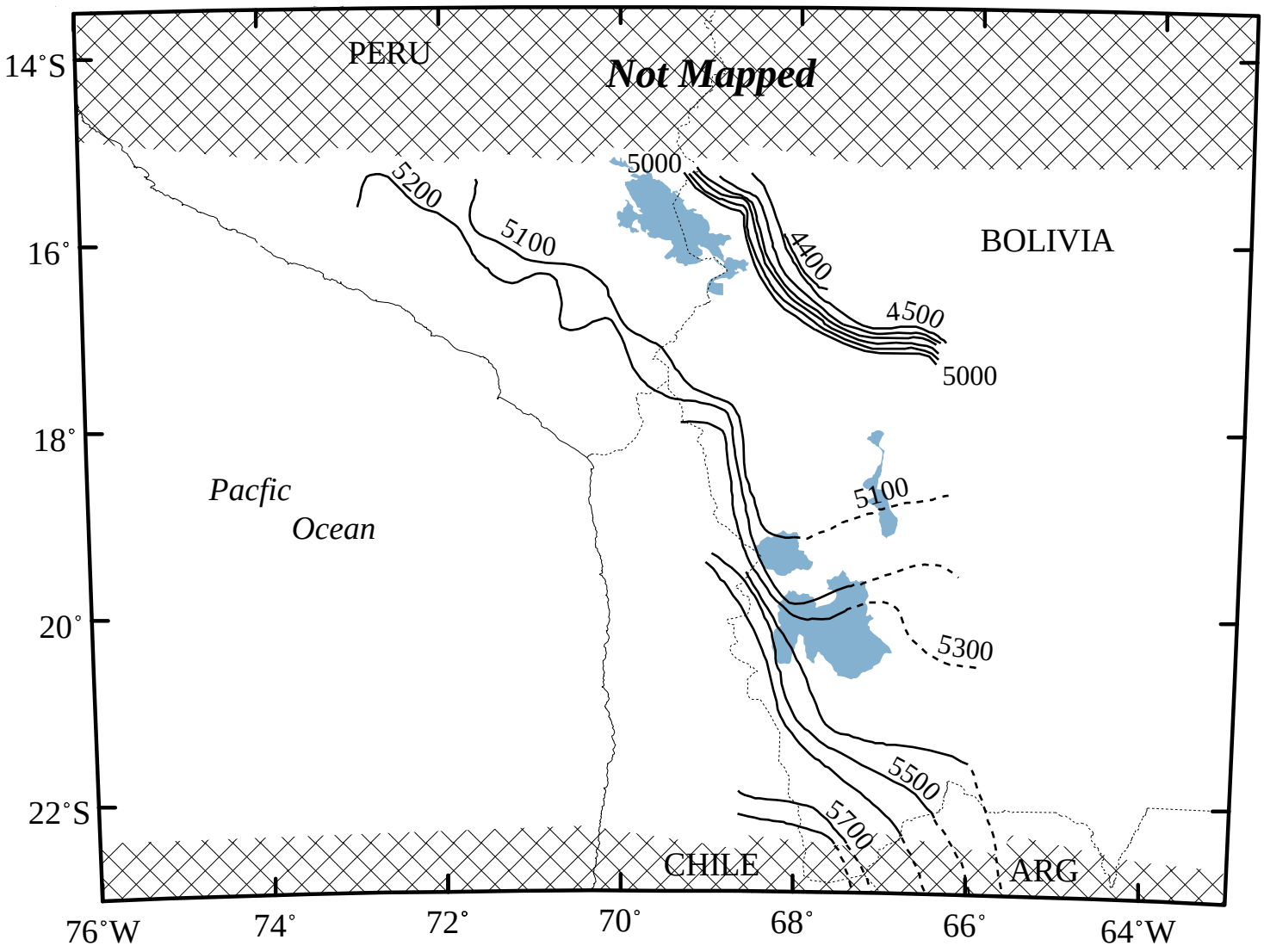
PERU
Not Mapped
BOLIVIA
Pacfic
Ocean
CHILE
ARG
5000
5200
5100
4400
4500
5000
5100
5300
5500
5700
14˚S
16˚
18˚
20˚
22˚S
76˚W
74˚
72˚
70˚
68˚
66˚
64˚W

Figure 3.10 late Pleistocene equilibrium line altitudes in the central Andes based on the glaciers shown in **Figure 3.6**. The contours were calculated by determining the minimum snowline elevation within a moving 0.25° x 0.25° moving window and then contouring. Contour interval is 200 m.

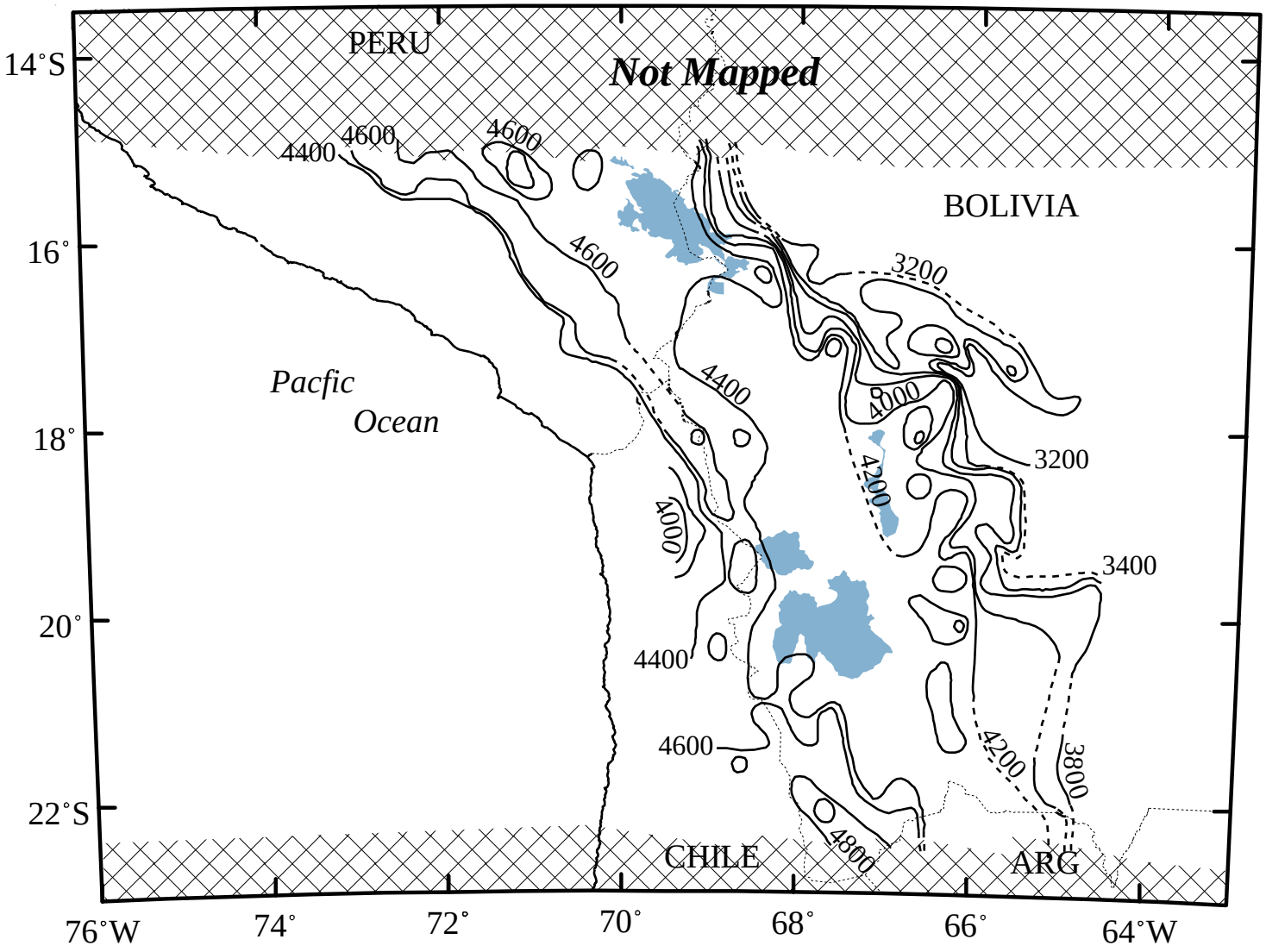
PERU
Not Mapped
BOLIVIA
Pacfic
Ocean
CHILE
ARG
14˚S
16˚
18˚
20˚
22˚S
76˚W
74˚
72˚
70˚
68˚
66˚
64˚W
4400
4600
4600
4600
4400
4000
4200
3200
3200
3400
4400
4600
4200
3800
4800

region (Kuhn, 1980). Late Pleistocene ELA also rose steeply across the eastern cordillera then gently rose southwest across the plateau to >4800 m in the western cordillera. In southwestern Peru and northern Chile, there was a slight drop in the elevations of the late Pleistocene equilibrium line along the western slopes of the western cordillera. Like modern glaciers in areas where the precipitation gradient is steep, such as along the eastern Cordillera in Bolivia, the late Pleistocene ELA rose quickly and where the east-west precipitation gradient is gentler, the rise in ELA was more gradual. This indicates that at the time of the local glacial maximum, precipitation in the central Andes had a predominately easterly source as today.

The equilibrium line of late Pleistocene glaciers was 500-1200 m lower than today (**Figure 3.11**). The lowering was greatest along the eastern cordillera of Peru and Bolivia where the ELA was consistently 1000-1200 lower than today. As discussed in detail in Chapter 1, this uniform depression is the best proxy for the late Pleistocene temperature change and is consistent with a 5-9°C cooling. A 1000 m or more lowering of the equilibrium line also occurred in the western cordillera. Presently the glaciers in this region are confined to extremely high altitudes and are thought to be much more sensitive to precipitation changes than to temperature changes (Kaser, 1995; Kuhn, 1980). The high sensitivity to precipitation changes makes a precipitation increase the most likely explanation for the large ELA lowering observed in this arid region as has been previously hypothesized (Hastenrath, 1971; Wright, 1983). Extensive

Figure 3.11: late Pleistocene ELA depression in the central Andes. The ELA depression was calculated by creating continuous surfaces of modern and late Pleistocene ELA surfaces based on the contours shown in **Figure 3.9** and **3.10**. The depression is a simple difference between the two that has been smoothed with a low pass filter to remove high frequency noise. Contour interval 100 m.

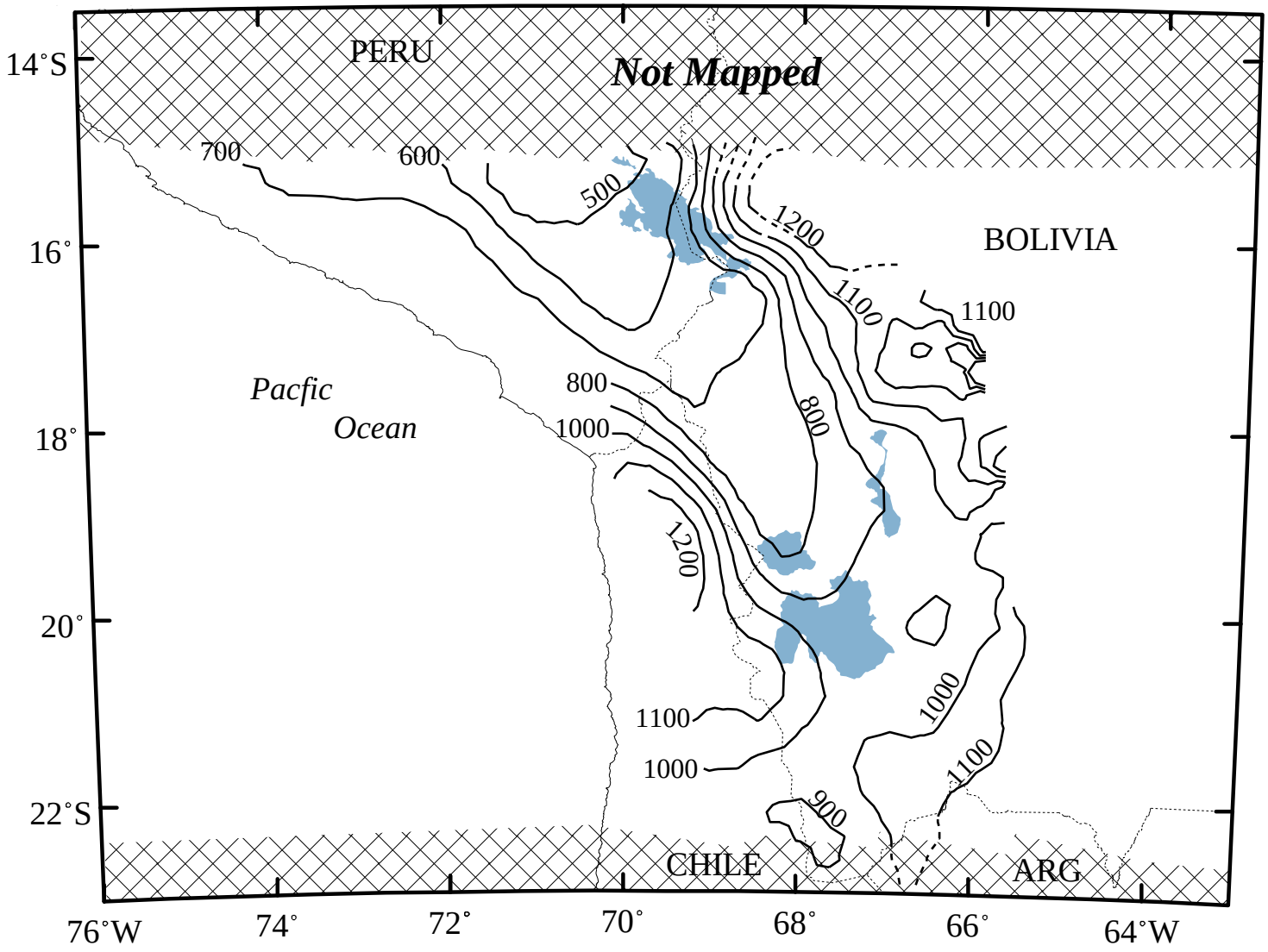
PERU
Not Mapped
BOLIVIA
Pacfic
Ocean
CHILE
ARG
700
600
500
1200
1100
1100
800
800
1000
1200
1100
1000
1000
1100
900
14˚S
16˚
18˚
20˚
22˚S
76˚W
74˚
72˚
70˚
68˚
66˚
64˚W

glacier expansion under much drier conditions (Fox, 1993; Satoh, 1979) is at odds with current understanding of modern glacier behavior in the region.

The actual ELA depression in the central Andes was considerably more complicated than the uniform 1000 m of depression often assumed for the tropics (Broecker and Denton, 1989; Rind and Peteet, 1985). ELA depression over much of the Altiplano was much less than 1000 m. Areas of southeast Peru and Bolivia experienced only a 500 to 800 m ELA lowering. These areas of

small ELA lowering correspond to areas of high elevation but low relief (**Figure 3.1**) and suggest that high plateaus limit the elevation to which glaciers could descend during the late Pleistocene. The coincidence of multiple phases of glaciation reaching nearly the same elevation along the western slope of the Cordillera Real, Bolivia (Argollo, 1980; Gouze *et al.*, 1986; Seltzer, 1992) is another indication that the Altiplano and other regions of high elevation but low relief cause a non-climatic threshold to limit glacier expansion. On these high plateaus, both in Peru and Bolivia, several small ice caps developed that were probably quite similar to the present Quelccaya Ice Cap in Peru. On Landsat TM, they are easily identified by their low relief and hummocky topography as well as the numerous kettle lakes left behind as the glaciers melted

Summary

The regional view provided by Landsat Thematic Mapper images provides an effective tool for identification and mapping of late Pleistocene glacial features in the semiarid central Andes. Simple radiometric and geometric corrections are all that are required to integrate multiple TM scenes into a single seamless mosaic that can be used for regional scale geomorphic mapping. The remote sensing techniques used here are equally applicable to mapping late Pleistocene glacier features in other remote semiarid environments such as the Tibetan Plateau and the Atlas mountains of north Africa. As the cost of using satellite images decreases and the spatial resolution increases, satellite images can only become more important in geomorphic studies.

Acknowledgments

This work is supported by the NASA mission to Planet Earth/Earth Observing System grant NAGW-2638 as well as support from the DOE Graduate Fellowship for Global Change Program. My thanks go to the present and former members of the Cornell Andes project, especially Eric Fielding and Timothy Gubbels, who helped make the Cornell University Landsat archive accessible to all. I also am indebted to James Aber for discussions on the subject. Glacier inventory data for Peru and Bolivia were kindly provided by W. Haeberli and M. Hoelzle of the World Glacier Monitoring Service.

Bibliography

Aber, J. S., Spellman, E. E., and Webster, M. P. (1993). Landsat Remote Sensing of Glacial Terrain. *In* "Glaciotectonics and Mapping Glacial Deposits: Proceedings of the INQUA Commission on Formation and Properties of Glacial Deposits." (J. S. Aber, Ed.), pp. 215-225, Canadian Plains Research Center, University of Regina.

Argollo, J. (1980). "Los pie de montes de la Cordillera Real Entre los valles de La Paz y de Tuni estudio geológico Pio-Cuaternaria." Unpublished Ph.D. thesis, Universidad Mayor San Andreas.

Bahr, D. B., Meier, M. F., and Peckham, S. D. (1995). The physical basis for glacier volume-area scaling and implications for mass balance profiles. *EOS* **76,** F208.

Broecker, W. S., and Denton, G. H. (1989). The role of ocean-atmosphere reorganizations in glacial cycles. *Geochimica et Cosmochimica Acta* **53,** 2465-2501.

Chavez, P. S. (1988). An improved dark-object subtraction technique for atmospheric scattering correction of multispectral data. *Remote Sensing of Environment* **24,** 459-479.

Chavez, P. S., Jr. (1989). Radiometric calibration of Landsat Thematic Mapper multispectral images. *Photogrammetric Engineering and Remote Sensing* **55,** 1285-1294.

Defense Mapping Agency. (1989). Digital Chart of the World Database (MIL-D-89009). U.S. Government Printing Office, Washington, D.C.

Dozier, J. (1989). Spectral signature of alpine snow cover from the Landsat Thematic Mapper. *Remote Sensing of Environment* **28,** 9-22.

Fox, A. N. (1993). "Snowline altitude and climate in the Central Andes (5-28°S) at present and during the Late Pleistocene Glacial Maximum." Unpublished Ph.D. thesis, Cornell University.

Gouze, P., Argollo, J., Saliege, J.-F., and Servant, M. (1986). Interprétation paléoclimatique des oscillations des glaciers au cours des 20 derniers millénaires dans les régions tropicals; exemple des Andes boliviennes. *Academie de Sciences* **303,** 219-223.

Hastenrath, S. (1971). On the Pleistocene snow-line depression in the arid regions of the South American Andes. *Journal of Glaciology* **10,** 225-267.

Hidrandina. (1988). Glacier Inventory of Peru. Consejo Nacional de Ciencia y Tecnologia (CONCYTEC), Huaraz.

Isacks, B. L. (1988). Uplift of the Central Andean Plateau and bending of the Bolivian Anticline. *Journal of Geophysical Research* **93,** 3211-3231.

Jordan, E. (1991). "Die Gletscher der bolivianischen Andean." Franz Steiner Verlag Stuttgart, Eurasburg, Germany.

Kaser, G. (1995). Some notes on the behavior of tropical glaciers. *Bull. Inst. fr. études andines* **24,** 671-681.

Kuhn, M. V. (1980). Vergletscherung, Nullgradgrenze und Niederschlag in den Anden. *In* "Jahrbuch des Sonnblickvereins, 1978-1979.", pp. 1-13. Springer Verlag, Wien.

Lillesand, T. M., and Kiefer, R. W. (1987). "Remote Sensing and Image Interpretation." John Wiley & Sons, New York.

Markham, B. L., and Barker, J. L. (1986). Landsat MSS and TM post-calibration dynamic ranges, exoatmospheric reflectances and at satellite temperatures. *EOSAT Technical Notes* **1,** 3-8.

Meier, M. F., and Bahr, D. B. (1995). Counting glaciers: use of scaling methods to estimate the number, size, and thickness distribution of the glaciers of the world. *EOS* **76,** F182.

Meierding, T. C. (1982). Late Pleistocene glacial equilibrium-line altitudes in the Colorado Front Range: a comparison of methods. *Quaternary Research* **18,** 289-310.

Mercer, J. H. (1984). Late Cainozoic glacial variations in South America south of the equator. *In* "Late Cainozoic Palaeoclimates of the Southern Hemisphere." (A. A. Balkema, Ed.), pp. 45-58.

Nogami, M. (1976). Altitude of the modern snowline and Pleistocene snowline in the Andes. *Tokyo Metropolitan University Geographical Reports* **11,** 71-86.

Oyarzun, C. G. (1987). Inventario do Glaciares de los Andes Chilenos desde los 18° a los 32° de Latitud Sur. *Revista de Geografia Norte Grande* **14,** 35-48.

Porter, S. (1985). Extent of Late Pleistocene glaciers in Afghanistan based on interpretation of Landsat imagery. *In* "Climate and Geology of Kashmir, the last 4 million years; proceedings of the international workshop on the Late Cenozoic palaeoclimatic changes in Kashmir and central Asia." (D. P. Argrawal, Ed.), pp. 191-195. Current Trends in Geology.

Rind, D., and Peteet, D. (1985). Terrestrial conditions at the Last Glacial Maximum and CLIMAP sea surface temperature estimates: are they consistent? *Quaternary Research* **24,** 1-22.

Robinove, C. J. (1982). Computation with physical values from Landsat digital data. *Photogrammetric Engineering and Remote Sensing* **48,** 781-784.

Satoh, H. (1979). On the Snow-line Altitude in the Central and Southern Andes of the Modern Age and the Diluvial Epoch. *In* "Paleolimnology of Lake Biwa and the Japanese Pleistocene." (S. Horie, Ed.), pp. 387-415.

Seltzer, G. O. (1990). Recent Glacial History and Paleoclimate of the Peruvian-Bolivian Andes. *Quaternary Science Reviews* **9,** 137-152.

Seltzer, G. O. (1992). Late Quaternary glaciation of the Cordillera Real, Bolivia. *Journal of Quaternary Science* **7,** 87-98.

Slater, P. N., Doyle, F. J., Fritz, N. L., and Weltch, R. (1983). Photographic systems for remote sensing. *In* "Second Edition of Manual of Remote Sensing." (R. N. Colwell, Ed.), pp. 231-291. American Society of Photogrammetry.

Williams, R. S. J. (1986). Glacier inventory of Iceland: Evaluation and use of sources of data. *Annals of Glaciology* **8,** 184-191.

Wright, H. E. (1983). Late-Pleistocene Glaciation and Climate Around the Junin Plain, Central Peruvian Highlands,. *Geografiska Annaler* **65 A,** 35-43.